The developmental hourglass model is applicable to the spinal cord

Katsuki Mukaigasa*, Chie Sakuma, Hiroyuki Yaginuma

Department of Neuroanatomy and Embryology, School of Medicine, Fukushima Medical University

*Correspondence: kamukaig@fmu.ac.jp

Summary

The developmental hourglass model predict that embryonic morphology is most conserved at mid-embryonic stage and diverge at early and late stage. This model is generally considered by whole embryonic level. Here, we demonstrate that the hourglass model is also applicable to the more reduced element, the spinal cord. In the middle of the spinal cord development, dorsoventrally arrayed neuronal progenitor domains are established, which is conserved among vertebrates. We found that, by comparing the single-cell transcriptomes between mice and zebrafish, V3 interneurons, a subpopulation of the post-mitotic spinal neurons, display the divergent molecular profiles. We also found non-conservation of *cis*-regulatory elements located around the progenitor fate determinants, indicating the rewiring of the upstream gene regulatory network. These results demonstrate that, despite the conservation of the progenitor domains, processes before and after the progenitor domain specification has diverged. This study may help understand the molecular basis of the developmental hourglass model.

Keywords

The developmental hourglass model, Single cell RNA-seq, *Cis* regulatory module, Gene regulatory network, Evolution, Spinal cord

Introduction

The vertebrate neural tube can produce a diverse array of neurons in a precisely controlled and reproducible manner. During neurogenesis and neuronal differentiation, each neuron is assigned a distinct feature such as neurotransmitter phenotype, axonal projection pathway, and cell body localization (Lai et al., 2016; Lu et al., 2015; Sagner and Briscoe, 2019). Initial phase of this process is the fate specification of progenitor cells, whereby molecularly defined progenitor domains are established with sharp boundary along the dorsoventral axis of the neural tube (Briscoe et al., 2000). Each progenitor identity is specified through highly complex gene regulatory network (GRN), which is composed of graded Shh signaling activity from ventral to dorsal, Bmp and Wnt signaling molecules expressed dorsally, pan-neural transcriptional activator Sox1-3, and a number of domain-specific transcription factors (TFs) functioning as repressor (Andrews et al., 2019; Balaskas et al., 2012; Delás and Briscoe, 2020; Kutejova et al., 2016; Nishi et al., 2015; Oosterveen et al., 2012; Peterson et al., 2012; Sagner and Briscoe, 2019; Zagorski et al., 2017). As the output of the GRN, 11 progenitor domains, termed dp1-6 in dorsal half, and p0, p1, p2, pMN and p3 in ventral half, are established (Lai et al., 2016; Lu et al., 2015; Sagner and Briscoe, 2019). Subsequently, multiple neuronal subtypes are generated from a single progenitor domain. For example, V2a, V2b and V2c interneurons (INs) are differentiated from p2 domain (Del Barrio et al., 2007; Li et al., 2005; Panayi et al., 2010; Peng et al., 2007), and dI1i and dI1c INs are differentiated from dp1 domain (Ding et al., 2012; Wilson et al., 2008).

Each subtype of post-mitotic neurons proceeds to the maturation process, such as migration, axon projection and circuit formation. These knowledges have been constructed mainly based on the chick and mouse studies, while a number of researches using zebrafish has demonstrated that the spatial architecture of the progenitor domains in the neural tube is largely conserved among vertebrate (Cheesman and Eisen, 2004; Cheesman et al., 2004; Gribble et al., 2007; Guner and Karlstrom, 2007; Lewis et al., 2005; Park et al., 2002; Schäfer et al., 2005).

However, there exist overt differences in the post-mitotic neuronal maturation between amniotes and teleost. For example, V2a INs, which is defined by the expression of Vsx2 (Chx10), contribute to the locomotor rhythm generation in zebrafish (Eklöf-Ljunggren et al., 2012), whereas V2a INs in mice play a role for the left-right alternation of limbs by providing excitatory input to the commissural INs (Crone et al., 2008, 2009). This implies that, during post-mitotic differentiation in mice and zebrafish, V2a INs are assigned the different properties, or are placed in different position within the spinal locomotor circuit (Kiehn, 2016). Another example is Robo3, an axon guidance receptor essential for commissural axons to cross the midline (Friocourt and Chédotal, 2017; Marillat et al., 2004; Sabatier et al., 2004). In the spinal cord of amniotes, Robo3 is expressed in V0, V1, and V3 INs in the ventral spinal cord, which encompass commissural INs (Friocourt et al., 2019; Tulloch et al., 2019). However, in zebrafish, although double labeling of *robo3* and neuronal subtype markers is not conducted, *robo3* expression is observed in the region encompassing MNs (Challa et al., 2005). If zebrafish MNs express *bona fide robo3*, differentiation of MN has diverged between amniotes and zebrafish, as MNs of amniotes never express Robo3 (Friocourt et al., 2019; Tulloch et al., 2019).

In addition to the post-mitotic differentiation, a process before the establishment of progenitor domains also differs in amniotes and zebrafish. *Shh* is essential gene for

74 specification of ventral neural tube, and are expressed in the notochord and floor plate in
75 amniotes (Echelard et al., 1993; Riddle et al., 1993; Roelink et al., 1994). In contrast, 3 *Shh*-
76 related genes, *shha* (*sonic hedgehog*), *shhb* (*tiggy winkle hedgehog*) and *ihhb* (*echidna*
77 *hedgehog*) are expressed in notochord and/or floor plate in zebrafish, conferring a functional
78 redundancy of hedgehog (Hh) signaling (Currie and Ingham, 1996; Ekker et al., 1995; Krauss
79 et al., 1993). The Hh signaling pathway culminates in Gli family TFs, which function as
80 transcriptional activator or repressor depending on Hh signaling activity (Briscoe and
81 Thérond, 2013). Amniote possess 3 *Gli* genes, *Gli1*, *Gli2* and *Gli3*, whereas teleost possess 4
82 *Gli* genes, *gli1*, *gli2a*, *gli2b* and *gli3*. Loss of function experiments of *Gli* genes lead to
83 apparently different phenotypes between mice and zebrafish. For example, *Gli1* knock-out
84 mice are viable and appear normal, showing that *Gli1* is not essential for embryogenesis in
85 mice (Park et al., 2000). In contrast, *gli1* mutant zebrafish display severe cranial motor
86 neuron deficiency, reduced Hh-target genes such as *ptch1* and *nkx2.2a*, and die at larval stage
87 (Chandrasekhar et al., 1999; Karlstrom et al., 1996, 2003). In *Gli2* knock-out mice, floor
88 plate is not specified, and MNs aberrantly occupy the ventral-most domain in the spinal cord,
89 though MN itself is differentiated (Ding et al., 1998; Matise et al., 1998), whereas in
90 zebrafish, *gli2a* is completely dispensable for normal embryogenesis and growth to adulthood
91 (Karlstrom et al., 2003; Vanderlaan et al., 2005; Wang et al., 2013), and *gli2b* knock-down
92 cause a marked reduction of MNs in the spinal cord (Ke et al., 2008). Knock-down of *gli3* in
93 zebrafish lead to the reduction of MNs (Vanderlaan et al., 2005), however, in *Gli3* mutant
94 mice, patterning defects of floor plate and MNs are not observed (Persson et al., 2002).
95 Overall, the processes before and after the progenitor domain specification have diverged
96 among vertebrates, despite the conservation of the dorsoventral arrangement of the progenitor
97 domains. This pattern of developmental divergence is highly consistent with the
98 developmental hourglass model, which argue that embryonic morphology at early and late

99 developmental stages are divergent and that at mid-embryonic stage is conserved (Duboule,
100 1994; Hu et al., 2017; Irie and Kuratani, 2014). However, the process of the spinal cord
101 development has never been investigated from the perspective of this model. Here, we
102 provide evidence supporting that the developmental hourglass model is applicable to the
103 spinal cord development. We examined the single-cell transcriptome data from mice and
104 zebrafish, and provide another example of diverse differentiation of the post-mitotic neuron.
105 We also examined the transcriptional regulatory elements in the neural tube patterning genes
106 based on ChIP-seq and ATAC-seq data and sequence conservation, suggesting that GRN
107 upstream to the progenitor domain specification has been rewired during vertebrate evolution.
108 Based on our findings and robust development of the neuronal progenitor specification
109 (Balaskas et al., 2012; Delás and Briscoe, 2020; Exelby et al., 2021; Xiong et al., 2013;
110 Zagorski et al., 2017), we propose that the progenitor domain configuration in the neural tube
111 is less evolvable due to its canalization (Waddington, 1942).
112

113 **Results**

114 *Two distinct subtypes of V3 INs in amniotes*

115 Neuronal subtypes repertoire of V3 INs, which are differentiated from ventral-most p3
116 progenitor domain, remain relatively unclear among spinal neurons both in amniotes and
117 teleosts. Thus, we focused on V3 IN to clarify to what extent the post mitotic neuronal
118 differentiation has diverged among vertebrates. We examined single-cell RNA-sequence
119 (scRNA-seq) data obtained from the spinal cord of mouse embryos (Delile et al., 2019). The
120 data consist of the whole spinal cord cells from embryonic day (E) 9.5 to E13.5. We extract
121 data having V3 IN profile (*Nkx2-2* or *Sim1* positive), and applied graph-based clustering and
122 dimensionality reduction by tSNE to these cells, and then the differentially expressed genes
123 in each cluster was identified (Table S1). Expression of several markers were visualized on

124 tSNE plots (Fig.1A). *Nkx2-2* is a marker of p3 progenitor domain and V3 INs (Briscoe et al.,
125 1999). *Sim1* is a post-mitotic V3 IN marker (Zhang et al., 2008). V3 INs are glutamatergic
126 neurons, thus express *Slc17a6* (*vGlut2*) (Zhang et al., 2008). Expression of *Sox2*, *Neurog3*
127 and *Tubb3* in this order indicate the transition from progenitor to differentiated neuron
128 (Carcagno et al., 2014), indicating that medial to lateral direction in the spinal cord
129 corresponds to top to bottom direction in this plot. We found at least two distinct populations
130 in V3 INs; one is positive for *Robo3*, *Olig3*, and *Cntn2* (*Tag1*) (cluster numbered 5 in Fig.1A),
131 and another is positive for *Lhx1* (cluster numbered 1 in Fig.1A, Table S1).

132 To distinguish these two subtypes *in vivo*, markers of each subtypes (*ROBO3* and LHX1)
133 are examined in the spinal cord of the chick embryo at Hamburger-Hamilton stage (HH) 25-
134 26 (Fig.1B-K). NKX2-2 is used as a marker of p3 progenitor domain and V3 INs. The post-
135 mitotic V3 INs are distinguished by the expression of *SIM1*. We found that the expression of
136 *ROBO3* is localized medially within the post-mitotic V3 INs. To confirm this further,
137 commissural axons passing through and bisecting the V3 INs were utilized as landmark.
138 Some V3 INs can be observed laterally to the commissural axons, however, these cells do not
139 express *ROBO3* (Fig.2F,G,K). Rather, *ROBO3* is expressed selectively by V3 INs located
140 medially to the commissural axons (Fig.2F,G). In contrast, LHX1 is expressed in the laterally
141 located population of the V3 INs (Fig.2H-J). These observations confirmed that two subtypes
142 of V3 INs found by scRNA-seq are spatially, and probably also functionally, distinct
143 populations in the developing spinal cord.

144

145 *Gene expression profile of V3 IN in zebrafish is distinct from that in amniotes*

146 Next, we analyzed the scRNA-seq data derived from zebrafish whole embryo at 1 and 2
147 day post fertilization (dpf) (Farnsworth et al., 2020) to determine whether V3 INs of zebrafish
148 are equivalent to those of amniotes. We extracted the data having the spinal cord profiles

149 (detailed procedure of the data subsetting is provided in Fig.S1). Similarly to the data
150 analysis of the mouse spinal cord, clustering and dimensionality reduction were applied
151 (Fig.2). In the tSNE plot, the progenitor cells, which mainly consist of 1 dpf cells, can be
152 identified by the expression of *sox3* and non-expression of *elavl3* (Fig.2, clusters numbered 0,
153 3, 4, 7, 11, 15, and 17). Expression of the domain specific TFs, such as *pax6b*, *olig2* and
154 *nkx2.2b*, were localized at the specific space in the tSNE plot, which is parallel to the
155 expression domain *in vivo* along the dorsoventral axis of the neural tube (Fig.2, Fig.S2).
156 These data also corroborate the evolutionary conservation of the progenitor domain
157 organization in the neural tube (Cheesman and Eisen, 2004; Cheesman et al., 2004; Gribble et
158 al., 2007; Guner and Karlstrom, 2007; Lewis et al., 2005; Park et al., 2002; Schäfer et al.,
159 2005). V3 INs can be distinguished by the expression of *sim1a* (magenta circle in Fig.2).
160 These V3 INs are *slc17a6b* positive glutamatergic neurons like amniotes. However, unlike
161 amniotes, almost all V3 INs express *robo3* in zebrafish, and there is no expression of *olig3*
162 and *cntn2*. The expression of *Lhx1* and *Robo3* is mutually exclusive in the amniotes, yet this
163 is not the case in the zebrafish. Furthermore, *neurog3*, one of the V3 IN specific TFs
164 (Carcagno et al., 2014), is not expressed in the V3 INs of zebrafish (Fig.2, compare to Fig.1).
165 These results indicate that V3 INs of zebrafish are not equivalent to those of amniotes so far
166 as the gene expressions are compared.
167
168 *CRM in Robo3 locus is not conserved in teleosts*
169 Focusing on *robo3* in zebrafish, *mnx1* positive MNs (black circle in Fig.2) also express
170 *robo3*. This is apparently different from amniotes, in which *Robo3* is never expressed in MNs
171 (Friocourt et al., 2019), implying that the transcriptional regulation of *Robo3* has diverged
172 during vertebrate evolution. To confirm this, we searched for the transcription regulatory
173 elements around *Robo3* locus using available ChIP-seq and ATAC-seq data of neural cells

174 (Fig.3). We found the putative *cis*-regulatory module (CRM) harboring multiple TF binding
175 sites with open chromatin state at around 20 kb upstream of *Robo3* transcription start site
176 (TSS) (Fig. 3, CRM in *Robo3* locus is abbreviated as *Robo3-CRM*). To confirm the function
177 of *Robo3-CRM*, reporter assay was performed using chick *in ovo* electroporation system. We
178 cloned *Robo3-CRM* from mouse genome into vector containing minimal promotor and *GFP*
179 (resulting construct is named *Robo3-CRM::GFP*). In the chick spinal cord after the
180 electroporation of *Robo3-CRM::GFP*, GFP expression was observed to overlap the
181 endogenous *ROBO3* expression, and GFP positive axons cross the midline (Fig.3). More
182 specifically, we found that GFP was expressed in LHX1 positive dorsal and intermediate INs,
183 EVX1 positive V0 INs, and NKX2-2 positive V3 INs, but not in ISL1 positive dI3 INs and
184 MNs, consistent with the endogenous *ROBO3* expressing cells (Fig.3) (Tulloch et al., 2019).
185 These results demonstrated that *Robo3-CRM* can recapitulate the normal expression pattern
186 of *Robo3* almost completely in the spinal cord.
187 Notably, when sequence conservation was checked using Multiz alignments in UCSC
188 genome browser among vertebrates, *Robo3-CRM* is conserved in tetrapods, but not in teleosts
189 (Fig.3). Weak conservation of *Robo3-CRM* is observed in spotted gar, a basal actinopterygian
190 (Fig.S3), suggesting that common ancestor of bony vertebrates possess *Robo3-CRM*, which
191 has been lost in teleost lineage (Lee et al., 2011). These results suggest that divergent
192 expression patterns of *robo3* in zebrafish is likely to be due to loss of *Robo3-CRM*. In
193 addition, it is also suggested that a part of axon guidance mechanisms in the post-mitotic
194 neurons might have diverged during vertebrate evolution.
195
196 *Non-conservation of GBSs in Gli1 and Ptch1 loci in vertebrates*
197 Next, we examined whether the upstream process before the progenitor fate specification
198 has also diverged among vertebrates. Previous studies have reported that the impacts of *Gli*

199 loss of function on the neuronal progenitors are different between mice and zebrafish
200 (Chandrasekhar et al., 1999; Karlstrom et al., 2003; Tyurina et al., 2005; Vanderlaan et al.,
201 2005; Wang et al., 2013). This raises the possibility that some Gli binding sites (GBSs), that
202 is, the sites of action of Hh signaling, varies among vertebrates. To test this, *Gli1* and *Ptch1*
203 loci were interrogated, as these genes are direct target of Hh signaling. We searched for GBS
204 in mouse genome and check the sequence conservation using Maltiz alignments in UCSC
205 genome browser. Using Gli1 and Gli3 ChIP-seq data, many GBSs were identified in mouse
206 *Gli1* and *Ptch1* loci near TSS and within intron (Fig.4), confirming previous report (Dai et al.,
207 1999; Nishi et al., 2015). ATAC-seq data confirmed that these GBSs are open chromatin state
208 in neural cells. We found that most of these GBSs are not conserved among vertebrates. In
209 the case of *Gli1*, clustered GBSs are conserved only in mammals, and in the *Ptch1* locus,
210 most GBSs are conserved only in tetrapods, but lost in teleosts (Fig.4, highlighted region).
211 These findings imply that GBS is highly evolvable element. This may partly explain the
212 discrepancy of the *Gli* loss of function phenotypes between mice and zebrafish.
213
214 *Non-conservation of CRMs of progenitor fate specifying TFs in vertebrates*
215 Since the regulatory elements in *Robo3*, *Gli1* and *Ptch1* are not conserved among
216 vertebrates, we expect that non-conservation of the regulatory elements can be found in other
217 genes. Thus, we applied the same analysis to TFs functioning as progenitor fate determinants
218 expressed in the neural tube. Indeed, we found that *Pax6-CRM*, *Gsx1-CRM*, *Dbx2-CRM*,
219 *Irx3-CRMs* (2 CRMs, designated *Irx3-CRM1* and *2*), and *Olig2-CRMs* (2 CRMs, designated
220 *Olig2-CRM1* and *2*) are conserved only in tetrapods, but lost in teleosts (Fig.5, highlighted
221 regions). These CRMs are open chromatin state in most cases, and are bound by Gli1, Gli3,
222 Sox2, Neurog2, Pax6, Pax7, Olig2, Nkx2-2 and Nkx6-1 in various combinations (Fig.5).
223 These TFs are essential components of GRN regulating the progenitor fate in the neural tube

224 (Balaskas et al., 2012; Delás and Briscoe, 2020; Exelby et al., 2021; Kutejova et al., 2016).
225 Thus, non-conservation of these CRMs and conservation of progenitor organization has
226 necessarily entailed the CRM turnover and GRN rewiring during vertebrate evolution. To
227 exclude the possibility that these CRMs has been lost due to having no functions, we carried
228 out the reporter assay by means of chick *in ovo* electroporation system. This experiment
229 confirmed that *Pax6-CRM*, *Gsx1-CRM*, *Dbx2-CRM*, *Irx3-CRM2*, and *Olig2-CRM2* functions
230 as enhancers in the neural tube cells, although more regulatory elements are needed to
231 precisely recapitulate the endogenous expression pattern (Fig.6). Note that this method
232 cannot capture the microRNA-based translational repression, which indeed affect the dorsal
233 boundary of Olig2 (Chen et al., 2011). The only exception is *Irx-CRM1*, which exert no
234 enhancer function in the chicken neural tube (data not shown). Enhancer function of *Olig2-*
235 *CRM1* was already validated previously (Exelby et al., 2021; Oosterveen et al., 2012;
236 Peterson et al., 2012; Wang et al., 2011). These results indicate that these CRMs are
237 functional in amniotes, but nevertheless, are lost in teleosts. This support the notion that the
238 progenitor fate specification system in the neural tube has undergone CRM turnover and
239 GRN rewiring during vertebrate evolution (Fig.7).
240

241 **Discussion**

242 *Divergent properties of post-mitotic neurons in vertebrates*

243 First, in this study, we compared the single-cell transcriptomes of mice and zebrafish to
244 elucidate the divergence of the post-mitotic neuronal differentiation. We found that, in
245 amniotes, V3 INs can be divided into two distinct subtypes. One is located medially and
246 express *Robo3*, *Olig3*, and *Cntn2*, and another is located laterally and express *Lhx1* (Fig.1).
247 We tried to make these V3 INs correspond with those of zebrafish, but it failed (Fig.1,2). This
248 indicates that V3 IN of amniotes is not equivalent to that of zebrafish at least regarding gene

249 expression profile, supporting the idea that the properties of post-mitotic neurons in the spinal
250 cord has diverged among vertebrates. This is in contrast to the case of progenitor cells, in
251 which each progenitor domains of zebrafish readily correspond with those of amniotes
252 (Fig.S2).

253 The role of V3 INs in mice is to secure the stable locomotor rhythm (Zhang et al., 2008).
254 Several studies also suggested that V3 INs is contribute to the left-right synchronous motor
255 output, such as gallop and bound (Danner et al., 2019; Kiehn, 2016; Rabe et al., 2009). These
256 gaits can be expressed by quadrupeds, but not by fishes. This suggests that the different
257 locomotor behavior between amniotes and teleosts is associated with the divergence of the
258 V3 IN property. The same may be the case with V2a INs, whose roles have diverged between
259 amniotes and teleosts (Azim et al., 2014; Crone et al., 2008, 2009; Eklöf-Ljunggren et al.,
260 2012; Kiehn, 2016). Given that the number of muscle and corresponding MNs has
261 significantly increased during tetrapod evolution, especially regarding limb muscles (Diogo
262 and Abdala, 2010), additional layer of neuronal circuits had been required to precisely control
263 complex locomotor behavior (Kiehn, 2016). This may be accomplished, at least in part, by
264 tinkering the already existing neuronal population (Jacob, 1977), eventually leading to the
265 divergence of the post-mitotic neuronal properties among vertebrates. Distinct expression
266 profiles of *Robo3* between amniotes and zebrafish may be one of the strategies for the
267 neuronal tinkering (Fig.1-3).

268

269 *Divergent processes leading to the conserved progenitor domains*

270 In the latter part of this study, we investigated the transcriptional regulatory elements
271 located around the progenitor fate specifying genes in order to reveal to what extent the
272 upstream process before the progenitor specification has diverged in vertebrates. In *Gli1*
273 locus, clustered GBSs near the TSS are conserved only in mammals, but not in teleosts

274 (Fig.4). Even in birds and reptiles, these GBSs are conserved only partially. Nevertheless,
275 *Gli1* is expressed in response to Hh signaling commonly in vertebrates (Aglyamova and
276 Agarwala, 2007; Karlstrom et al., 2003; Luo et al., 2006), suggesting the presence of distinct
277 GBSs with equivalent function. Actually, zebrafish possesses 3 GBSs in *Gli1* locus, which
278 are conserved only in a part of teleost species (Wang et al., 2013), indicating that regions
279 where Hh signaling is eventually transduced has shifted during vertebrate evolution. This is
280 supported by the similar situation in *Ptch1* locus (Fig.4) (Wang et al., 2013). Bicoid is a
281 morphogen playing a crucial role for the patterning of the anterior-posterior axis in
282 *Drosophila* blastoderm, and there are fundamental similarities between Bicoid and Shh
283 (Briscoe and Small, 2015). It is noteworthy that Bicoid binding sites has also undergone rapid
284 turnover in *Diptera* (McGregor et al., 2001). Flexibility of morphogen response elements
285 might contribute to the integration of the morphogen dependency into the patterning system
286 of the embryo (Dearden and Akam, 1999; Miyamoto and Wada, 2013; Ren et al., 2020;
287 Stauber et al., 1999).

288 In *Pax6*, *Gsx1*, *Dbx2*, *Irx3*, and *Olig2* loci in mouse genome, we identified functional
289 CRMs bound by multiple TFs (Fig.5,6). These CRMs are conserved only in tetrapods, but
290 lost in teleosts (Fig.5). Given that the progenitor domain organization is conserved among
291 vertebrates, these findings indicate the CRM turnover and GRN rewiring during vertebrate
292 evolution (Fig.7). This is considered as a case of developmental system drift (DSD) (True and
293 Haag, 2001). Several studies have reported similar situation, in which divergent regulatory
294 sequences in different species result in the conserved gene expressions (Barrière et al., 2012;
295 Fisher et al., 2006; Hare et al., 2008; Ludwig et al., 1998, 2000; Paris et al., 2013; Stolfi et al.,
296 2014; Swanson et al., 2011). In these cases including the present study, GRN architecture is
297 likely to be maintained as a whole despite the CRM turnover, as demonstrated in mammalian
298 evolution (Stergachis et al., 2014; Vierstra et al., 2014).

299 The process of the neural tube formation is different between amniotes and zebrafish also
300 morphogenetically. In amniotes, a midline groove is formed by bending of the neural plate,
301 and then the edges of the neural plate are fused, making the neural tube (Schoenwolf and
302 Smith, 1990). On the other hand, in zebrafish, the solid neural keel with no central canal is
303 formed by convergent movement of the neural plate cells, and then the central canal opens
304 secondarily (Schmitz et al., 1993). Taken together, the neural tube formation is a case of DSD
305 from both genetic and morphogenetic viewpoints.
306
307 *Molecular basis of the hourglass model in the spinal cord*
308 Altogether, our results demonstrate that divergence of the developmental process of the
309 spinal cord is in accordance with the developmental hourglass model. Then, what impose the
310 hourglass-like pattern on the evolution of the spinal cord development? We discuss about it as
311 follows. The progenitor regionalization in the neural tube is highly robust developmental
312 system, and thus is insensitive against noises and mutations (Balaskas et al., 2012; Delás and
313 Briscoe, 2020; Exelby et al., 2021; Xiong et al., 2013; Zagorski et al., 2017). Simulation
314 study also propose that the developmental system robustness is an emergent property of the
315 complex GRN (Bergman and Siegal, 2003; von Dassow et al., 2000; Siegal and Bergman,
316 2002), supporting indirectly the robustness of the neuronal progenitor specification system,
317 which is organized by highly complex GRN (Kutejova et al., 2016). From the evolutionary
318 perspective, such a robust (canalized) developmental system can accommodate genetic
319 variations without disturbing the development (Rutherford and Lindquist, 1998; Waddington,
320 1942). In other words, the progenitor specification system in the neural tube is buffering the
321 genetic variations. We speculate that this situation had consequently led to the CRM turnover
322 and GRN rewiring, while the progenitor arrangement was maintained. Once cells are released
323 from the progenitor domains as post-mitotic neurons, individual neurons depend on the

mechanisms regulating post-mitotic maturation which is distinct from the progenitor specification GRN. As mentioned before, maturation process is considered to diverge in association with locomotor divergence. Eventually, through vertebrate evolution, developmental divergence of the spinal cord might become the hourglass shape. The present study only considers the spinal cord. Thus, it is of particular interest to examine whether this scenario is also the case in other developmental systems or even in whole embryonic level.

More importantly, if partial modification is admitted, neuroectodermal regionalization is conserved beyond vertebrates among bilaterians (Arendt, 2018; Denes et al., 2007; Jung and Dasen, 2015). This suggest that developmental system robustness of the neuroectodermal regionalization had already been acquired in common ancestor of bilaterians, and upstream signals of the neuroectodermal regionalization had been modified after divergence of phyla (e.g., Hh signalling recruitment in deuterostomes) (Miyamoto and Wada, 2013; Ren et al., 2020). This is supported by the notion of the common origin of the central nervous system (CNS) in bilateria (Arendt, 2018; Denes et al., 2007), but is inconsistent with the convergent evolution of CNS (Martín-Durán et al., 2018).

Acknowledgements

We thank Y. Watanabe and T. Shimada for technical supports. This work was supported by JSPS KAKENHI Grant Number 18K14718 and 18K06835. Computations were partially performed on the NIG supercomputer at ROIS National Institute of Genetics. The monoclonal antibodies 74.5A5, 4F2, 3A10, 99.1-3A2, PAX6, and GFP-G1, developed by T. M. Jessell, J. Dodd, S. Brenner-Morton, A. Kawakami, J. R. Sanes, and M. Yamagata were obtained from the Developmental Studies Hybridoma Bank, created by the NICHD of the NIH and maintained at The University of Iowa, Department of Biology, Iowa City, IA 52242.

349 **Author Contributions**

350 Conceptualization, K.M.; Methodology, K.M.; Formal Analysis, K.M.; Investigation,
351 K.M. and C.S.; Writing - Original Draft, K.M.; Writing - Review & Editing, K.M and H.Y.;
352 Funding Acquisition, K.M. and H.Y.

353

354 **Declaration of Interests**

355 The authors declare no competing interests.

356

357 **Figure Legends**

358 **Figure 1. Two distinct subtypes of V3 INs in amniotes**

359 (A) tSNE plot showing the cells with V3 IN identity derived from mouse embryonic
360 spinal cord. Expression levels of genes indicated are visualized on the tSNE plot. Top right
361 panel shows the result of graph-based clustering with each cluster being colored differently.
362 Cluster numbers (0-11) are labeled. Middle right panel shows embryonic day when cells are
363 corrected. There are 2 distinct clusters within the post-mitotic V3 INs; one is positive for
364 *Robo3*, *Olig3*, and *Cntn2* (cluster numbered 5), and another is positive for *Lhx1* (cluster
365 numbered 1). (B-K) Expressions of NKX2-2, *SIM1* and *ROBO3* are examined in the chick
366 spinal cord at the forelimb level at HH25-26. Growing axons are also visualized by
367 monoclonal antibody 3A10. Staining of *in situ* hybridization and immunohistochemistry is
368 colored by blue and brown, respectively. C, E and G show the enlarged views of the boxed
369 area in B, D, and F, respectively. (H-J) Immunohistochemistry using NKX2-2 and LHX1
370 antibodies. (K) Immunohistochemistry using NKX2-2 and 3A10 antibodies. Ventral-most
371 region of the spinal cord is shown in H-K. Scale bar: 100 μm in F for B, D and F, in K for H-
372 K.

373

374 **Figure 2. Gene expression profile of V3 IN in zebrafish is distinct from that in amniotes**

375 tSNE plot showing the cells with spinal cord identity derived from zebrafish embryos (1
376 and 2 dpf). Top left panel shows the result of graph-based clustering with each cluster being
377 colored differently. Cluster numbers (0-18) are labeled. Top right panel shows embryonic day
378 when cells are corrected. Left-most panel in second row shows progenitors and post-mitotic
379 neurons by distinct color. D and V indicate dorsal and ventral, respectively. Other panels
380 show the expression levels of genes indicated. Magenta and black circle indicate V3 INs and
381 MNs, respectively.

382

383 **Figure 3. CRM in *Robo3* locus is not conserved in teleosts**

384 (A) ChIP-seq and ATAC-seq peak call results are displayed in UCSC genome browser
385 with Multiz Alignments track. *Robo3* locus in mouse genome (mm10) is displayed. Region
386 harboring multiple TF binding sites (*Robo3-CRM*) is highlighted by magenta. Maltiz
387 Alignment track of tatrapods and teleosts are highlighted by different colors. (B-I) *Robo3-*
388 *CRM::GFP* was electroporated into chick neural tube. (B,C) Expression of GFP and *ROBO3*
389 was examined at HH20 (B) and HH25 (C) after electroporation. GFP expression overlapped
390 with the endogenous *ROBO3* expression. (D-I) Expression of GFP and TFs indicated was
391 examined at HH25 after electroporation. Scale bar: 100 μm in C for B and C, in I for D-I.

392

393 **Figure 4. Non-conservation of GBSs in *Gli1* and *Ptch1* loci in vertebrates**

394 Gli1/3 ChIP-seq and ATAC-seq peak call results are displayed in UCSC genome browser
395 with Multiz Alignments track. *Gli1* and *Ptch1* loci in mouse genome (mm10) are shown. In
396 *Gli1* locus, region highlighted by magenta indicates the open chromatin region which is
397 bound by Gli1/3, and is conserved only in mammals. Maltiz Alignment track of mammals
398 and non-mammals are highlighted by different colors. In *Ptch1* locus, regions highlighted by

399 magenta indicates the open chromatin regions which are bound by Gli1/3, and are conserved
400 only in tetrapods. Maltiz Alignment track of tatrapods and teleosts are highlighted by
401 different colors.
402
403 **Figure 5. Non-conservation of CRMs of progenitor fate specifying TFs in vertebrates**
404 ChIP-seq and ATAC-seq peak call results are displayed in UCSC genome browser with
405 Multiz Alignments track (display mode is dense). Mouse *Pax6*, *Gsx1*, *Dbx2*, *Irx3* and *Olig2*
406 loci are displayed. Regions harboring multiple TF binding sites (CRMs) are highlighted by
407 magenta, which are conserved only in tetrapods. In *Irx3* and *Olig2* loci, two distinct CRMs
408 are numbered 1 and 2 under the track. In *Pax6*, *Dbx2* and *Olig2* loci, previously validated
409 CRMs are indicated by open triangle under the track (Oosterveen et al., 2012; Peterson et al.,
410 2012).
411
412 **Figure 6. Enhancer functions of CRMs of progenitor fate specifying TFs**
413 CRM reporter vectors indicated are electroporated into chick neural tube together with
414 CAGGS::mCherry as control vector. (A-J) GFP and mCherry expression were examined at
415 HH19-20 in the forelimb level neural tube. (K-O) The endogenous expression of genes
416 indicated were examined by *in situ* hybridization (L,M,N) or immunohistochemistry (K,O)
417 together with GFP expression. These 5 CRMs display enhancer functions, though GFP
418 expression domains incompletely overlap with endogenous expression domain. *Pax6-CRM*
419 induces GFP expression almost ubiquitously, yet the expression is not observed in the roof
420 plate (A,F,K). *Gsx1-CRM* induces GFP expression in the dorsal neural tube, but does not
421 induce in the more ventral region than the endogenous expression domain (B,G,L). GFP
422 expression domain induced by *Dbx2-CRM* overlap with the endogenous expression domain
423 almost completely (C,H,M). It is also the case with *Irx3-CRM2* (D,I,N). *Olig2-CRM* induces

424 the GFP expression in the intermediate to ventral region, which partially overlap with, but is
425 more dorsal than, the endogenous expression domain (E,J,O). Scale bar: 100 μm.
426
427 **Figure 7. The hourglass-like pattern of the developmental divergence of the spinal cord**
428 Summary of the present study is shown. In this drawing, development proceed from
429 bottom to top. Only 5 progenitor domains are set up for simplification. Bottom drawing
430 represents the GRNs regulating the progenitor domain establishment. CRMs (indicated by
431 open boxes) located in the progenitor fate specifying genes (GeneA-D) has diverged
432 (turnover) between amniotes and teleosts. Accordingly, these GRNs have been rewired,
433 which is considered as DSD. Nevertheless, these distinct GRNs result in the same progenitor
434 domain organization due to the developmental system robustness. Top drawing represents the
435 divergence of the differentiation process of the post-mitotic neuron. After individual cells
436 leave the progenitor domains as post-mitotic neurons, some neurons undergo distinct
437 maturation process between amniotes and teleosts. Thus, there exist neuronal subpopulations
438 whose function is different between amniotes and teleosts.
439
440 **Methods**
441 *Experimental animals*
442 Fertilized chicken eggs were obtained from Takeuchi farm (Nara, Japan) and incubated
443 at 38°C in a humidified incubator. Embryos were staged according to Hamburger-Hamilton
444 stage series (Hamburger and Hamilton, 1951). All animal experiments were performed in
445 accordance with the Rules of Fukushima Medical University Animal Experiments, with
446 approval of the Animal Experiments Committee of Fukushima Medical University (approval
447 number 2020103).
448

449 *scRNA-seq data analysis*

450 Mouse spinal cord scRNA-seq data (Delile et al., 2019) was obtained from ArrayExpress
451 (accession number E-MTAB-7320). UMI count matrix was generated using Cell Ranger
452 version 3.1.0 (10x Genomics). In this step, normalization was skipped in order to maximize
453 sensitivity (cellranger aggr was executed with --normalize=none). The output matrix was
454 feed into Seurat (R package) version 3.1.5 (Butler et al., 2018). Zebrafish whole embryo
455 scRNA-seq data (Farnsworth et al., 2020) was obtained as Seurat object (.rds file) from Dr.
456 Miller's website (https://www.adammillerlab.com/resources-1). Detailed procedure of
457 normalization, data subsetting, graph-based clustering, and dimensionality reduction using
458 Seurat is provided in https://github.com/kmukaigasa/Spinalcord_MouseZebrafish.

459

460 *ChIP-seq data analysis*

461 ChIP-seq data were obtained from NCBI sequence read archive (SRA). Accession
462 numbers are as follows; GSE66961 for Pax6 (Sun et al., 2015), GSE42132 for Sox2, Gli1
463 (Peterson et al., 2012), GSE61673 for Gli3, Nkx2-2, Nkx6-1, Olig2 (Nishi et al., 2015),
464 GSE114172 for Neurog2 (Aydin et al., 2019), GSE87180 for Pax7 (Mayran et al., 2018). Cell
465 types used are embryonic forebrain (Pax6), AtT-20 cell (Pax7), and neural cells differentiated
466 from mouse ES cells (Sox2, Gli1/3, Nkx2-2, Nkx6-1, Olig2, Neurog2). Sequencing adaptors
467 and low quality bases was trimmed by Trimmomatic (version 0.39). FastQC (version 0.11.9)
468 was used for sequence quality check. Read mapping to mouse reference genome (mm10) was
469 performed by Bowtie2 (version 2.3.5) with default setting. Reads with low mapping quality
470 (MAPQ < 10) were removed by samtools (version 1.9). Peak call was performed by MACS2
471 (version 2.2.6). Output bedGraph file was converted to BigWig format by bdg2bw
472 (https://gist.github.com/jl32587/34370c995460f9d5ad65). BigWig track was visualized in
473 UCSC genome browser.

474

475 *ATAC-seq data analysis*

476 ATAC-seq data (Metzis et al., 2018) were obtained from ArrayExpress (E-MTAB-6337).
477 From the dataset, data of the neural progenitor cells with spinal cord identity were used. Read
478 quality control was done as ChIP-seq. Read mapping was performed by Bowtie2 with
479 following parameters; -X 2000 --sensitive-local. PCR duplicates were marked using Picard
480 (version 2.9.2). Reads with low mapping quality (MAPQ < 30) were removed by samtools.
481 Peak call was performed by MACS2 with following parameters; -f BAMPE -g mm -q 0.05 --
482 nomodel --keep-dup auto -B.

483

484 *Comparison of genomic sequence by VISTA*

485 For interspecies comparison of genomic sequence, partial genomic sequences were
486 obtained from UCSC genome browser (https://genome.ucsc.edu) and Ensembl
487 (https://www.ensembl.org/index.html), and VISTA (Frazer et al., 2004) are used to align and
488 visualize the results.

489

490 *Vector construction*

491 For RNA probe preparation, partial fragment of *ROBO3*, *IRX3*, *DBX2*, and *GSX1* was
492 amplified by PCR from chick embryonic spinal cord cDNA. Primer sequences used are
493 provided in Table S2. The fragments were inserted into pCR-XL-TOPO (Thermo Fisher) or
494 *pBluescriptKS*. For reporter assay of CRMs, genomic DNA fragments were amplified by
495 PCR from solution which was prepared by digesting tail tip of C57BL/6J mouse. The
496 amplified fragments were inserted into *pSF-pA-MinProm-eGFP* vector (Oxford genetics).
497 Positions of CRMs within the mouse reference genome are provided in Table S3. For
498 construction of *pCAGGS-mCherry*, *mCherry* gene cassette of *pmCherry-C1* (Clontech) was

499 inserted into *pCAGGS* (Niwa et al., 1991).

500

501 *in ovo electroporation*

502 A small window was opened on the top of the fertilized chicken egg shell. The electrodes
503 were placed on both sides of the neural tube of HH12-13 chick embryo. Plasmid DNA was
504 injected into the neural tube. During injection, electric pulses (25 V, 50 ms, 5 times, 950 ms
505 interval) were applied using CUY21EDIT (BEX, Tokyo, Japan). Plasmids were prepared at 1
506 μg/μl for *pSF-Robo3-CRM::GFP*, 20-50 ng/μl for *pSF-Pax6-CRM::GFP*, *pSF-Gsx1-*
507 *CRM::GFP*, *pSF-Dbx2-CRM::GFP*, *pSF-Irx3-CRM::GFP*, *pSF-Olig2-CRM::GFP*, 0.5 ng/μl
508 for *pCAGGS-mCherry*.

509

510 *Immunohistochemistry*

511 Embryos were fixed in 0.1 M phosphate buffer / 4% paraformaldehyde (PFA) at room
512 temperature for 45-60 min or 4°C overnight. Fixed embryos were cryoprotected in 20%
513 sucrose at 4°C overnight, embedded in OCT compound, and cryosectioned. In case of
514 overnight fixed samples, sections were boiled for 20 min in sodium citrate buffer (10 mM
515 sodium citrate, 0.05% Tween 20, pH 6.0) and cooled down to room temperature. After
516 washing with phosphate-buffered saline (PBS) containing 0.1% Triton X-100 (PBST), the
517 sections were incubated with primary antibodies at 4°C overnight, washed with PBST three
518 times for 5 min, and incubated with secondary antibodies for 1-2 h at room temperature. After
519 washing with PBST three times for 5 min, slides were coverslipped in VECTASHIELD
520 (Vector laboratories). The antibodies used are described in Table S4. In the case of anti-Pax6
521 and anti-Lhx1, Can Get Signal (TOYOBO, NKB-401) was used for diluent instead of PBST.
522 Images were captured using an Olympus BX51 fluorescent microscope equipped with an
523 Olympus DP71 digital camera, or an Olympus FluoView FV1000 confocal microscope.

524

525 *in situ hybridization*

526 For double staining of immunohistochemistry and *in situ* hybridization,
527 immunohistochemistry was performed as describe above with primary and secondary
528 antibody incubation being for 1 h at room temperature, and signal was developed by
529 VECTASTAIN Elite ABC kit (Vector laboratories), and then, proceed to the process of *in situ*
530 hybridization as described below. Plasmid for RNA probe template was linearized, and DIG-
531 labeled RNA probes were generated using DIG RNA labeling mix (Sigma-Aldrich,
532 11277073910) and T3 RNA polymerase (Promega, P2083).

533 Tissue slides were washed with PBS for 5 min, treated with protainaseK (2μg/ml) for 10
534 min, washed with PBS for 5min, fixed in 4% PFA for 10 min, and washed three times with
535 PBS for 5 min. The slides were then incubated in acetylation solution (100 mM
536 triethanolamine, pH 8.0) twice for 2-3 min, transferred in new acetylation solution and
537 acetylated for 15 min by adding dropwise acetic anhydride (0.3% final concentration), and
538 washed with PBS three times for 5 min. The slides were prehybridized with hybridization
539 buffer (50% formamide, 5X SSC, 5X Denhardt's, 500 μg/ml herring sperm DNA, 250 μg/ml
540 yeast RNA) for 2-3h at room temperature, and hybridized with hybridization buffer
541 containing DIG-labelled RNA probe. The slides were coverslipped and incubated in
542 humidified chamber at 70°C overnight. The following day, slides were transferred in 5X SSC
543 at 70°C for 5 min, washed twice in 0.2X SSC for 30 min at 70°C, and washed in 0.2X SSC
544 for 30 min at room temperature. Slides were washed with buffer B1 (100mM Tris-HCl pH
545 7.5, 150 mM NaCl, 0.1% Tween 20) three times for 30 min, incubated with buffer B1
546 containing 10% heat-inactivated normal goat serum for 2-3h at room temperature, and then
547 incubated with buffer B1 containing alkaline phosphatase conjugated anti-DIG antibody
548 (Roche 11093274910, 1:5000) and 1% heat-inactivated normal goat serum at 4°C overnight.

549 The following day, slides were washed 5 times with buffer B1 for 30 min, and incubated in
550 buffer B3 (100 mM Tris-HCl pH 9.5, 100 mM NaCl, 50 mM MgCl2, 0.1% Tween20) three
551 times for 5 min. Slides were incubated with BM purple (Roche, 11442074001) until the
552 signal was visualized (3 h to overnight). After that, slides were washed three times with
553 buffer B1 for 30 min, then washed three times with PBS for 5min, and coverslipped in
554 Fluoromount (Diagnostic Biosystems, K024).
555

556 **References**

557 Aglyamova, G. V., and Agarwala, S. (2007). Gene expression analysis of the Hedgehog
558 signaling cascade in the chick midbrain and spinal cord. Dev. Dyn. *236*, 1363–1373.
559 Andrews, M.G., Kong, J., Novitch, B.G., and Butler, S.J. (2019). New perspectives on the
560 mechanisms establishing the dorsal-ventral axis of the spinal cord. Curr. Top. Dev. Biol. *132*,
561 417–450.
562 Arendt, D. (2018). Animal Evolution: Convergent Nerve Cords? Curr. Biol. *28*, R225–R227.
563 Aydin, B., Kakumanu, A., Rossillo, M., Moreno-Estellés, M., Garipler, G., Ringstad, N.,
564 Flames, N., Mahony, S., and Mazzoni, E.O. (2019). Proneural factors Ascl1 and Neurog2
565 contribute to neuronal subtype identities by establishing distinct chromatin landscapes. Nat.
566 Neurosci. *22*, 897–908.
567 Azim, E., Jiang, J., Alstermark, B., and Jessell, T.M. (2014). Skilled reaching relies on a V2a
568 propriospinal internal copy circuit. Nature *508*, 357–363.
569 Balaskas, N., Ribeiro, A., Panovska, J., Dessaud, E., Sasai, N., Page, K.M., Briscoe, J., and
570 Ribes, V. (2012). Gene regulatory logic for reading the Sonic Hedgehog signaling gradient in
571 the vertebrate neural tube. Cell *148*, 273–284.
572 Barrière, A., Gordon, K.L., and Ruvinsky, I. (2012). Coevolution within and between
573 Regulatory Loci Can Preserve Promoter Function Despite Evolutionary Rate Acceleration.

574 PLoS Genet. *8*, e1002961.
575 Bergman, A., and Siegal, M.L. (2003). Evolutionary capacitance as a general feature of
576 complex gene networks. Nature *424*, 549–552.
577 Briscoe, J., and Small, S. (2015). Morphogen rules: design principles of gradient-mediated
578 embryo patterning. Development *142*, 3996–4009.
579 Briscoe, J., and Thérond, P.P. (2013). The mechanisms of Hedgehog signalling and its roles
580 in development and disease. Nat. Rev. Mol. Cell Biol. *14*, 418–431.
581 Briscoe, J., Sussel, L., Serup, P., Hartigan-O'Connor, D., Jessell, T.M., Rubenstein, J.L.R.,
582 and Ericson, J. (1999). Homeobox gene Nkx2.2 and specification of neuronal identity by
583 graded Sonic hedgehog signalling. Nature *398*, 622–627.
584 Briscoe, J., Pierani, A., Jessell, T., and Ericson, J. (2000). A homeodomain protein code
585 specifies progenitor cell identity and neuronal fate in the ventral neural tube. Cell *101*, 435–
586 445.
587 Butler, A., Hoffman, P., Smibert, P., Papalexi, E., and Satija, R. (2018). Integrating single-
588 cell transcriptomic data across different conditions, technologies, and species. Nat.
589 Biotechnol. *36*, 411–420.
590 Carcagno, A.L., Di Bella, D.J., Goulding, M., Guillemot, F., and Lanuza, G.M. (2014).
591 Neurogenin3 Restricts Serotonergic Neuron Differentiation to the Hindbrain. J. Neurosci. *34*,
592 15223–15233.
593 Challa, A.K., McWhorter, M.L., Wang, C., Seeger, M.A., and Beattie, C.E. (2005). Robo3
594 isoforms have distinct roles during zebrafish development. Mech. Dev. *122*, 1073–1086.
595 Chandrasekhar, A., Schauerte, H.E., Haffter, P., and Kuwada, J.Y. (1999). The zebrafish
596 detour gene is essential for cranial but not spinal motor neuron induction. Development *126*,
597 2727–2737.
598 Cheesman, S.E., and Eisen, J.S. (2004). Gsh1 Demarcates Hypothalamus and Intermediate

599 Spinal Cord in Zebrafish. Gene Expr. Patterns *5*, 107–112.

600 Cheesman, S.E., Layden, M.J., Von Ohlen, T., Doe, C.Q., and Eisen, J.S. (2004). Zebrafish
601 and fly Nkx6 proteins have similar CNS expression patterns and regulate motoneuron
602 formation. Development *131*, 5221–5232.

603 Chen, J.A., Huang, Y.P., Mazzoni, E.O., Tan, G.C., Zavadil, J., and Wichterle, H. (2011).
604 Mir-17-3p Controls Spinal Neural Progenitor Patterning by Regulating Olig2/Irx3 Cross-
605 Repressive Loop. Neuron *69*, 721–735.

606 Crone, S.A., Quinlan, K.A., Zagoraiou, L., Droho, S., Restrepo, C.E., Lundfald, L., Endo, T.,
607 Setlak, J., Jessell, T.M., Kiehn, O., et al. (2008). Genetic Ablation of V2a Ipsilateral
608 Interneurons Disrupts Left-Right Locomotor Coordination in Mammalian Spinal Cord.
609 Neuron *60*, 70–83.

610 Crone, S.A., Zhong, G., Harris-Warrick, R., and Sharma, K. (2009). In mice lacking V2a
611 interneurons, gait depends on speed of locomotion. J. Neurosci. *29*, 7098–7109.

612 Currie, P.D., and Ingham, P.W. (1996). Induction of a specific muscle cell type by a
613 hedgehog-like protein in zebrafish. Nature *382*, 452–455.

614 Dai, P., Akimaru, H., Tanaka, Y., Maekawa, T., Nakafuku, M., and Ishii, S. (1999). Sonic
615 Hedgehog-induced Activation of the Gli1 Promoter Is Mediated by GLI3. J. Biol. Chem. *274*,
616 8143–8152.

617 Danner, S.M., Zhang, H., Shevtsova, N.A., Borowska-Fielding, J., Deska-Gauthier, D.,
618 Rybak, I.A., and Zhang, Y. (2019). Spinal V3 Interneurons and Left–Right Coordination in
619 Mammalian Locomotion. Front. Cell. Neurosci. *13*, 1–23.

620 von Dassow, G., Meir, E., Munro, E.M., and Odell, G.M. (2000). The segment polarity
621 network is a robust developmental module. Nature *406*, 188–192.

622 Dearden, P., and Akam, M. (1999). Developmental evolution: Axial patterning in insects.
623 Curr. Biol. *9*, R591-4.

624 Del Barrio, M.G., Taveira-Marques, R., Muroyama, Y., Yuk, D.-I., Li, S., Wines-Samuelson,
625 M., Shen, J., Smith, H.K., Xiang, M., Rowitch, D., et al. (2007). A regulatory network
626 involving Foxn4, Mash1 and delta-like 4/Notch1 generates V2a and V2b spinal interneurons
627 from a common progenitor pool. Development *134*, 3427–3436.
628 Delás, M.J., and Briscoe, J. (2020). Repressive interactions in gene regulatory networks:
629 When you have no other choice. Curr. Top. Dev. Biol. *139*, 239–266.
630 Delile, J., Rayon, T., Melchionda, M., Edwards, A., Briscoe, J., and Sagner, A. (2019). Single
631 cell transcriptomics reveals spatial and temporal dynamics of gene expression in the
632 developing mouse spinal cord. Development *146*, dev173807.
633 Denes, A.S., Jékely, G., Steinmetz, P.R.H., Raible, F., Snyman, H., Prud'homme, B., Ferrier,
634 D.E.K., Balavoine, G., and Arendt, D. (2007). Molecular Architecture of Annelid Nerve Cord
635 Supports Common Origin of Nervous System Centralization in Bilateria. Cell *129*, 277–288.
636 Ding, Q., Motoyama, J., Gasca, S., Mo, R., Sasaki, H., Rossant, J., and Hui, C.C. (1998).
637 Diminished Sonic hedgehog signaling and lack of floor plate differentiation in Gli2 mutant
638 mice. Development *125*, 2533–2543.
639 Ding, Q., Joshi, P.S., Xie, Z. -h., Xiang, M., and Gan, L. (2012). BARHL2 transcription
640 factor regulates the ipsilateral/contralateral subtype divergence in postmitotic dI1 neurons of
641 the developing spinal cord. Proc. Natl. Acad. Sci. U. S. A. *109*, 1566–1571.
642 Diogo, R., and Abdala, V. (2010). Muscles of vertebrates : comparative anatomy, evolution,
643 homologies and development (CRC Press).
644 Duboule, D. (1994). Temporal colinearity and the phylotypic progression: a basis for the
645 stability of a vertebrate Bauplan and the evolution of morphologies through heterochrony.
646 Development *1994*, 135–142.
647 Echelard, Y., Epstein, D.J., St-Jacques, B., Shen, L., Mohler, J., McMahon, J.A., and
648 McMahon, A.P. (1993). Sonic hedgehog, a member of a family of putative signaling

649 molecules, is implicated in the regulation of CNS polarity. Cell *75*, 1417–1430.
650 Ekker, S.C., Ungar, A.R., Greenstein, P., von Kessler, D.P., Porter, J.A., Moon, R.T., and
651 Beachy, P.A. (1995). Patterning activities of vertebrate hedgehog proteins in the developing
652 eye and brain. Curr. Biol. *5*, 944–955.
653 Eklöf-Ljunggren, E., Haupt, S., Ausborn, J., Dehnisch, I., Uhlén, P., Higashijima, S., and El
654 Manira, A. (2012). Origin of excitation underlying locomotion in the spinal circuit of
655 zebrafish. Proc. Natl. Acad. Sci. U. S. A. *109*, 5511–5516.
656 Exelby, K., Herrera-Delgado, E., Garcia Perez, L., Perez-Carrasco, R., Sagner, A., Metzis, V.,
657 Sollich, P., and Briscoe, J. (2021). Precision of Tissue Patterning is Controlled by Dynamical
658 Properties of Gene Regulatory Networks. Development dev.197566.
659 Farnsworth, D.R., Saunders, L.M., and Miller, A.C. (2020). A single-cell transcriptome atlas
660 for zebrafish development. Dev. Biol. *459*, 100–108.
661 Fisher, S., Grice, E.A., Vinton, R.M., Bessling, S.L., and McCallion, A.S. (2006).
662 Conservation of RET regulatory function from human to zebrafish without sequence
663 similarity. Science *312*, 276–279.
664 Frazer, K.A., Pachter, L., Poliakov, A., Rubin, E.M., and Dubchak, I. (2004). VISTA:
665 computational tools for comparative genomics. Nucleic Acids Res. *32*, W273–W279.
666 Friocourt, F., and Chédotal, A. (2017). The Robo3 receptor, a key player in the development,
667 evolution, and function of commissural systems. Dev. Neurobiol. *77*, 876–890.
668 Friocourt, F., Kozulin, P., Belle, M., Suárez, R., Di-Poï, N., Richards, L.J., Giacobini, P., and
669 Chédotal, A. (2019). Shared and differential features of Robo3 expression pattern in amniotes.
670 J. Comp. Neurol. *527*, 2009–2029.
671 Gribble, S.L., Nikolaus, O.B., and Dorsky, R.I. (2007). Regulation and function of Dbx genes
672 in the zebrafish spinal cord. Dev. Dyn. *236*, 3472–3483.
673 Guner, B., and Karlstrom, R.O. (2007). Cloning of zebrafish nkx6.2 and a comprehensive

674 analysis of the conserved transcriptional response to Hedgehog/Gli signaling in the zebrafish
675 neural tube. Gene Expr. Patterns *7*, 596–605.
676 Hamburger, V., and Hamilton, H.L. (1951). A series of normal stages in the development of
677 the chick embryo. J. Morphol. *88*, 49–92.
678 Hare, E.E., Peterson, B.K., Iyer, V.N., Meier, R., and Eisen, M.B. (2008). Sepsid even-
679 skipped enhancers are functionally conserved in Drosophila despite lack of sequence
680 conservation. PLoS Genet. *4*.
681 Hu, H., Uesaka, M., Guo, S., Shimai, K., Lu, T.-M., Li, F., Fujimoto, S., Ishikawa, M., Liu,
682 S., Sasagawa, Y., et al. (2017). Constrained vertebrate evolution by pleiotropic genes. Nat.
683 Ecol. Evol. *1*, 1722–1730.
684 Irie, N., and Kuratani, S. (2014). The developmental hourglass model: a predictor of the basic
685 body plan? Development *141*, 4649–4655.
686 Jacob, F. (1977). Evolution and tinkering. Science *196*, 1161–1166.
687 Jung, H., and Dasen, J.S. (2015). Evolution of Patterning Systems and Circuit Elements for
688 Locomotion. Dev. Cell *32*, 408–422.
689 Karlstrom, R.O., Trowe, T., Klostermann, S., Baier, H., Brand, M., Crawford, A.D.,
690 Grunewald, B., Haffter, P., Hoffmann, H., Meyer, S.U., et al. (1996). Zebrafish mutations
691 affecting retinotectal axon pathfinding. Development *123*, 427–438.
692 Karlstrom, R.O., Tyurina, O. V., Kawakami, A., Nishioka, N., Talbot, W.S., Sasaki, H., and
693 Schier, A.F. (2003). Genetic analysis of zebrafish gli1 and gli2 reveals divergent
694 requirements for gli genes in vertebrate development. Development *130*, 1549–1564.
695 Ke, Z., Kondrichin, I., Gong, Z., and Korzh, V. (2008). Combined activity of the two Gli2
696 genes of zebrafish play a major role in Hedgehog signaling during zebrafish
697 neurodevelopment. Mol. Cell. Neurosci. *37*, 388–401.
698 Kiehn, O. (2016). Decoding the organization of spinal circuits that control locomotion. Nat.

699 Rev. Neurosci. *17*, 224–238.

700 Krauss, S., Concordet, J.P., and Ingham, P.W. (1993). A functionally conserved homolog of
701 the Drosophila segment polarity gene hh is expressed in tissues with polarizing activity in
702 zebrafish embryos. Cell *75*, 1431–1444.

703 Kutejova, E., Sasai, N., Shah, A., Gouti, M., and Briscoe, J. (2016). Neural Progenitors
704 Adopt Specific Identities by Directly Repressing All Alternative Progenitor Transcriptional
705 Programs. Dev. Cell *36*, 639–653.

706 Lai, H.C., Seal, R.P., and Johnson, J.E. (2016). Making sense out of spinal cord
707 somatosensory development. Development *143*, 3434–3448.

708 Lee, A.P., Kerk, S.Y., Tan, Y.Y., Brenner, S., and Venkatesh, B. (2011). Ancient Vertebrate
709 Conserved Noncoding Elements Have Been Evolving Rapidly in Teleost Fishes. Mol. Biol.
710 Evol. *28*, 1205–1215.

711 Lewis, K.E., Bates, J., and Eisen, J.S. (2005). Regulation of iro3 expression in the zebrafish
712 spinal cord. Dev. Dyn. *232*, 140–148.

713 Li, S., Misra, K., Matise, M.P., and Xiang, M. (2005). Foxn4 acts synergistically with Mash1
714 to specify subtype identity of V2 interneurons in the spinal cord. Proc. Natl. Acad. Sci. U. S.
715 A. *102*, 10688–10693.

716 Lu, D.C., Niu, T., and Alaynick, W.A. (2015). Molecular and cellular development of spinal
717 cord locomotor circuitry. Front. Mol. Neurosci. *8*, 1–18.

718 Ludwig, M.Z., Patel, N.H., and Kreitman, M. (1998). Functional analysis of eve stripe 2
719 enhancer evolution in Drosophila, rules governing conservation and change. Development
720 *125*, 949–958.

721 Ludwig, M.Z., Bergman, C., Patel, N.H., and KreLtman, M. (2000). Evidence for stabilizing
722 selection in a eukaryotic enhancer element. Nature *403*, 564–567.

723 Luo, J., Ju, M.J., and Redies, C. (2006). Regionalized cadherin-7 expression by radial glia is

724 regulated by Shh and Pax7 during chicken spinal cord development. Neuroscience *142*,
725 1133–1143.
726 Marillat, V., Chédotal, A., Sabatier, C., Failli, V., Matsunaga, E., Sotelo, C., and Tessier-
727 Lavigne, M. (2004). The slit receptor Rig-1/Robo3 controls midline crossing by hindbrain
728 precerebellar neurons and axons. Neuron *43*, 69–79.
729 Martín-Durán, J.M., Pang, K., Børve, A., Lê, H.S., Furu, A., Cannon, J.T., Jondelius, U., and
730 Hejnol, A. (2018). Convergent evolution of bilaterian nerve cords. Nature *553*, 45–50.
731 Matise, M.P., Epstein, D.J., Park, H.L., Platt, K.A., and Joyner, A.L. (1998). Gli2 is required
732 for induction of floor plate and adjacent cells, but not most ventral neurons in the mouse
733 central nervous system. Development *125*, 2759–2770.
734 Mayran, A., Khetchoumian, K., Hariri, F., Pastinen, T., Gauthier, Y., Balsalobre, A., and
735 Drouin, J. (2018). Pioneer factor Pax7 deploys a stable enhancer repertoire for specification
736 of cell fate. Nat. Genet. *50*, 259–269.
737 McGregor, A.P., Shaw, P.J., Hancock, J.M., Bopp, D., Hediger, M., Wratten, N.S., and
738 Dover, G.A. (2001). Rapid restructuring of bicoid-dependent hunchback promoters within
739 and between Dipteran species: implications for molecular coevolution. Evol. Dev. *3*, 397–407.
740 Metzis, V., Steinhauser, S., Pakanavicius, E., Gouti, M., Stamataki, D., Ivanovitch, K.,
741 Watson, T., Rayon, T., Mousavy Gharavy, S.N., Lovell-Badge, R., et al. (2018). Nervous
742 System Regionalization Entails Axial Allocation before Neural Differentiation. Cell *175*,
743 1105-1118.e17.
744 Miyamoto, N., and Wada, H. (2013). Hemichordate neurulation and the origin of the neural
745 tube. Nat. Commun. *4*, 2713.
746 Nishi, Y., Zhang, X., Jeong, J., Peterson, K.A., Vedenko, A., Bulyk, M.L., Hide, W.A., and
747 McMahon, A.P. (2015). A direct fate exclusion mechanism by Sonic hedgehog-regulated
748 transcriptional repressors. Development *142*, 3286–3293.

749 Niwa, H., Yamamura, K., and Miyazaki, J. (1991). Efficient selection for high-expression
750 transfectants with a novel eukaryotic vector. Gene *108*, 193–199.
751 Oosterveen, T., Kurdija, S., Alekseenko, Z., Uhde, C.W., Bergsland, M., Sandberg, M.,
752 Andersson, E., Dias, J.M., Muhr, J., and Ericson, J. (2012). Mechanistic Differences in the
753 Transcriptional Interpretation of Local and Long-Range Shh Morphogen Signaling. Dev. Cell
754 *23*, 1006–1019.
755 Panayi, H., Panayiotou, E., Orford, M., Genethliou, N., Mean, R., Lapathitis, G., Li, S.,
756 Xiang, M., Kessaris, N., Richardson, W.D., et al. (2010). Sox1 is required for the
757 specification of a novel p2-derived interneuron subtype in the mouse ventral spinal cord. J.
758 Neurosci. *30*, 12274–12280.
759 Paris, M., Kaplan, T., Li, X.Y., Villalta, J.E., Lott, S.E., and Eisen, M.B. (2013). Extensive
760 Divergence of Transcription Factor Binding in Drosophila Embryos with Highly Conserved
761 Gene Expression. PLoS Genet. *9*, e1003748.
762 Park, H.C., Mehta, A., Richardson, J.S., and Appel, B. (2002). Olig2 Is Required for
763 Zebrafish Primary Motor Neuron and Oligodendrocyte Development. Dev. Biol. *248*, 356–
764 368.
765 Park, H.L., Bai, C., Platt, K.A., Matise, M.P., Beeghly, A., Hui, C.C., Nakashima, M., and
766 Joyner, A.L. (2000). Mouse Gli1 mutants are viable but have defects in SHH signaling in
767 combination with a Gli2 mutation. Development *127*, 1593–1605.
768 Peng, C.Y., Yajima, H., Burns, C.E., Zon, L.I., Sisodia, S.S., Pfaff, S.L., and Sharma, K.
769 (2007). Notch and MAML Signaling Drives Scl-Dependent Interneuron Diversity in the
770 Spinal Cord. Neuron *53*, 813–827.
771 Persson, M., Stamataki, D., Welscher, P. Te, Andersson, E., Böse, J., Rüther, U., Ericson, J.,
772 and Briscoe, J. (2002). Dorsal-ventral patterning of the spinal cord requires Gli3
773 transcriptional repressor activity. Genes Dev. *16*, 2865–2878.

774 Peterson, K.A., Nishi, Y., Ma, W., Vedenko, A., Shokri, L., Zhang, X., McFarlane, M.,
775 Baizabal, J.-M., Junker, J.P., van Oudenaarden, A., et al. (2012). Neural-specific Sox2 input
776 and differential Gli-binding affinity provide context and positional information in Shh-
777 directed neural patterning. Genes Dev. *26*, 2802–2816.
778 Prince, V.E., Moens, C.B., Kimmel, C.B., and Ho, R.K. (1998a). Zebrafish hox genes:
779 expression in the hindbrain region of wild-type and mutants of the segmentation gene,
780 valentino. Development *125*, 393–406.
781 Prince, V.E., Joly, L., Ekker, M., and Ho, R.K. (1998b). Zebrafish hox genes: genomic
782 organization and modified colinear expression patterns in the trunk. Development *125*, 407–
783 420.
784 Rabe, N., Gezelius, H., Vallstedt, A., Memic, F., and Kullander, K. (2009). Netrin-1-
785 dependent spinal interneuron subtypes are required for the formation of left-right alternating
786 locomotor circuitry. J. Neurosci. *29*, 15642–15649.
787 Ren, Q., Zhong, Y., Huang, X., Leung, B., Xing, C., Wang, H., Hu, G., Wang, Y., Shimeld,
788 S.M., and Li, G. (2020). Step-wise evolution of neural patterning by Hedgehog signalling in
789 chordates. Nat. Ecol. Evol. *4*, 1247–1255.
790 Riddle, R.D., Johnson, R.L., Laufer, E., and Tabin, C. (1993). Sonic hedgehog mediates the
791 polarizing activity of the ZPA. Cell *75*, 1401–1416.
792 Roelink, H., Augsburger, A., Heemskerk, J., Korzh, V., Norlin, S., Ruiz i Altaba, A., Tanabe,
793 Y., Placzek, M., Edlund, T., and Jessell, T.M. (1994). Floor plate and motor neuron induction
794 by vhh-1, a vertebrate homolog of hedgehog expressed by the notochord. Cell *76*, 761–775.
795 Rutherford, S.L., and Lindquist, S. (1998). Hsp90 as a capacitor for morphological evolution.
796 Nature *396*, 336–342.
797 Sabatier, C., Plump, A.S., Le Ma, Brose, K., Tamada, A., Murakami, F., Lee, E.Y.-H.P., and
798 Tessier-Lavigne, M. (2004). The divergent Robo family protein rig-1/Robo3 is a negative

799 regulator of slit responsiveness required for midline crossing by commissural axons. Cell *117*,
800 157–169.
801 Sagner, A., and Briscoe, J. (2019). Establishing neuronal diversity in the spinal cord: a time
802 and a place. Development *146*, dev182154.
803 Schäfer, M., Kinzel, D., Neuner, C., Schartl, M., Volff, J.N., and Winkler, C. (2005).
804 Hedgehog and retinoid signalling confines nkx2.2b expression to the lateral floor plate of the
805 zebrafish trunk. Mech. Dev. *122*, 43–56.
806 Schmitz, B., Papan, C., and Campos-Ortega, J.A. (1993). Neurulation in the anterior trunk
807 region of the zebrafish Brachydanio rerio. Roux's Arch. Dev. Biol. *202*, 250–259.
808 Schoenwolf, G.C., and Smith, J.L. (1990). Mechanisms of neurulation: Traditional viewpoint
809 and recent advances. Development *109*, 243–270.
810 Siegal, M.L., and Bergman, A. (2002). Waddington's canalization revisited: developmental
811 stability and evolution. Proc. Natl. Acad. Sci. U. S. A. *99*, 10528–10532.
812 Stauber, M., Jäckle, H., and Schmidt-Ott, U. (1999). The anterior determinant bicoid of
813 Drosophila is a derived Hox class 3 gene. Proc. Natl. Acad. Sci. U. S. A. *96*, 3786–3789.
814 Stergachis, A.B., Neph, S., Sandstrom, R., Haugen, E., Reynolds, A.P., Zhang, M., Byron, R.,
815 Canfield, T., Stelhing-Sun, S., Lee, K., et al. (2014). Conservation of trans-acting circuitry
816 during mammalian regulatory evolution. Nature *515*, 365–370.
817 Stolfi, A., Lowe, E.K., Racioppi, C., Ristoratore, F., Brown, C.T., Swalla, B.J., and
818 Christiaen, L. (2014). Divergent mechanisms regulate conserved cardiopharyngeal
819 development and gene expression in distantly related ascidians. Elife *3*, e03728.
820 Sun, J., Rockowitz, S., Xie, Q., Ashery-Padan, R., Zheng, D., and Cvekl, A. (2015).
821 Identification of in vivo DNA-binding mechanisms of Pax6 and reconstruction of Pax6-
822 dependent gene regulatory networks during forebrain and lens development. Nucleic Acids
823 Res. *43*, 6827–6846.

824 Swanson, C.I., Schwimmer, D.B., and Barolo, S. (2011). Rapid evolutionary rewiring of a
825 structurally constrained eye enhancer. Curr. Biol. *21*, 1186–1196.
826 True, J.R., and Haag, E.S. (2001). Developmental system drift and flexibility in evolutionary
827 trajectories. Evol. Dev. *3*, 109–119.
828 Tulloch, A.J., Teo, S., Carvajal, B. V., Tessier-Lavigne, M., and Jaworski, A. (2019). Diverse
829 spinal commissural neuron populations revealed by fate mapping and molecular profiling
830 using a novel Robo3Cre mouse. J. Comp. Neurol. *527*, 2948–2972.
831 Tyurina, O. V., Guner, B., Popova, E., Feng, J., Schier, A.F., Kohtz, J.D., and Karlstrom, R.O.
832 (2005). Zebrafish Gli3 functions as both an activator and a repressor in Hedgehog signaling.
833 Dev. Biol. *277*, 537–556.
834 Vanderlaan, G., Tyurina, O. V., Karlstrom, R.O., and Chandrasekhar, A. (2005). Gli function
835 is essential for motor neuron induction in zebrafish. Dev. Biol. *282*, 550–570.
836 Vierstra, J., Rynes, E., Sandstrom, R., Zhang, M., Canfield, T., Hansen, R.S., Stehling-Sun,
837 S., Sabo, P.J., Byron, R., Humbert, R., et al. (2014). Mouse regulatory DNA landscapes
838 reveal global principles of cis-regulatory evolution. Science *346*, 1007–1012.
839 Waddington, C.H. (1942). Canalization of development and the inheritance of acquired
840 characters. Nature *150*, 563–565.
841 Wang, H., Lei, Q., Oosterveen, T., Ericson, J., and Matise, M.P. (2011). Tcf/lef repressors
842 differentially regulate shh-gli target gene activation thresholds to generate progenitor
843 patterning in the developing CNS. Development *138*, 3711–3721.
844 Wang, X., Zhao, Z., Muller, J., Iyu, A., Khng, A.J., Guccione, E., Ruan, Y., and Ingham, P.W.
845 (2013). Targeted inactivation and identification of targets of the Gli2a transcription factor in
846 the zebrafish. Biol. Open *2*, 1203–1213.
847 Wilson, S.I., Shafer, B., Lee, K.J., and Dodd, J. (2008). A Molecular Program for
848 Contralateral Trajectory: Rig-1 Control by LIM Homeodomain Transcription Factors.

Neuron *59*, 413–424.

Xiong, F., Tentner, A.R., Huang, P., Gelas, A., Mosaliganti, K.R., Souhait, L., Rannou, N., Swinburne, I.A., Obholzer, N.D., Cowgill, P.D., et al. (2013). Specified neural progenitors sort to form sharp domains after noisy Shh signaling. Cell *153*, 550–561.

Zagorski, M., Tabata, Y., Brandenberg, N., Lutolf, M.P., Tkačik, G., Bollenbach, T., Briscoe, J., and Kicheva, A. (2017). Decoding of position in the developing neural tube from antiparallel morphogen gradients. Science *356*, 1379–1383.

Zhang, Y., Narayan, S., Geiman, E., Lanuza, G.M., Velasquez, T., Shanks, B., Akay, T., Dyck, J., Pearson, K., Gosgnach, S., et al. (2008). V3 Spinal Neurons Establish a Robust and Balanced Locomotor Rhythm during Walking. Neuron *60*, 84–96.

Figure 1

A

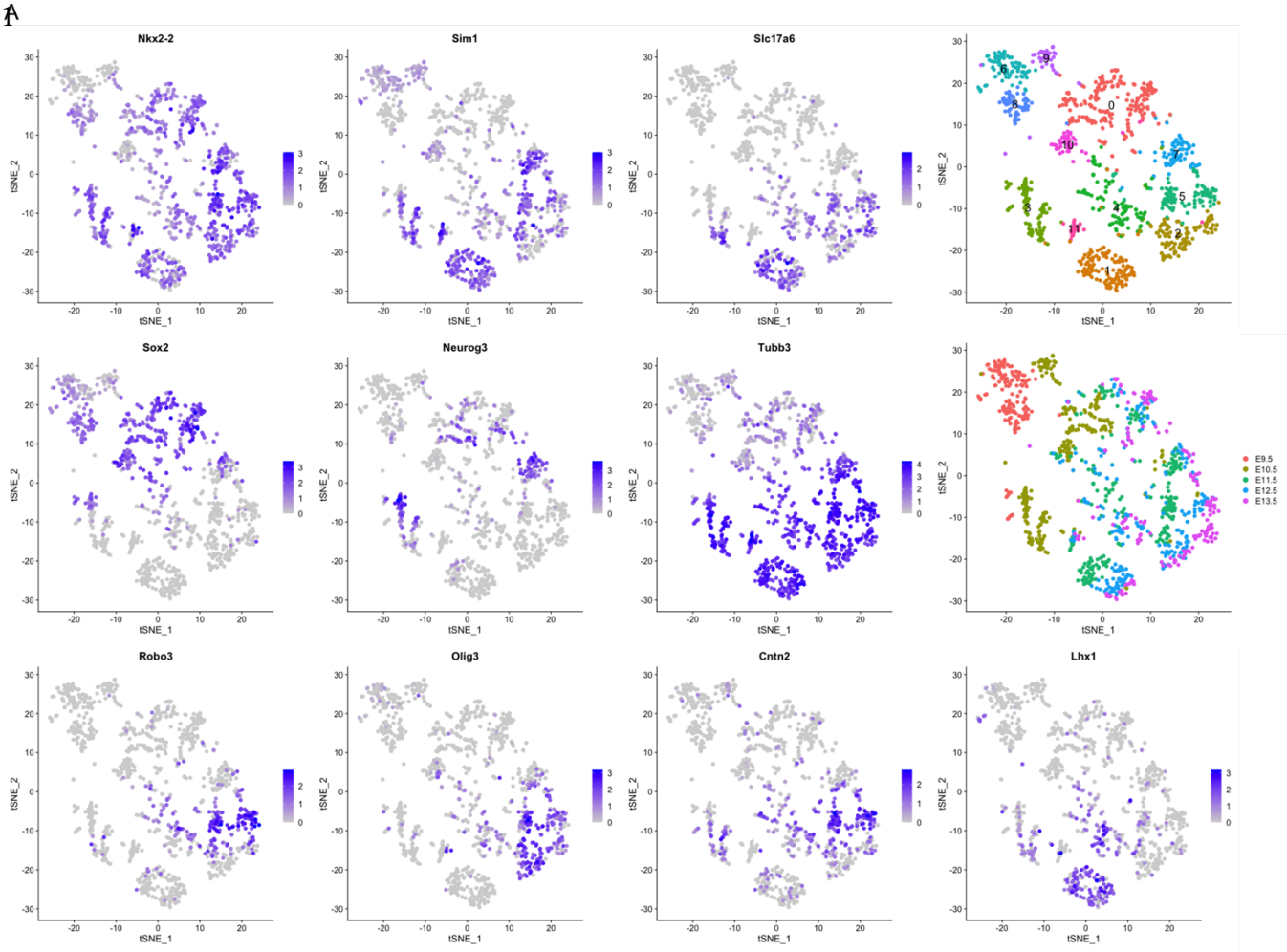
Nkx2-2
Sim1
Slc17a6
Sox2
Neurog3
Tubb3
Robo3
Olig3
Cntn2
Lhx1
tSNE_1
tSNE_2
E9.5
E10.5
E11.5
E12.5
E13.5

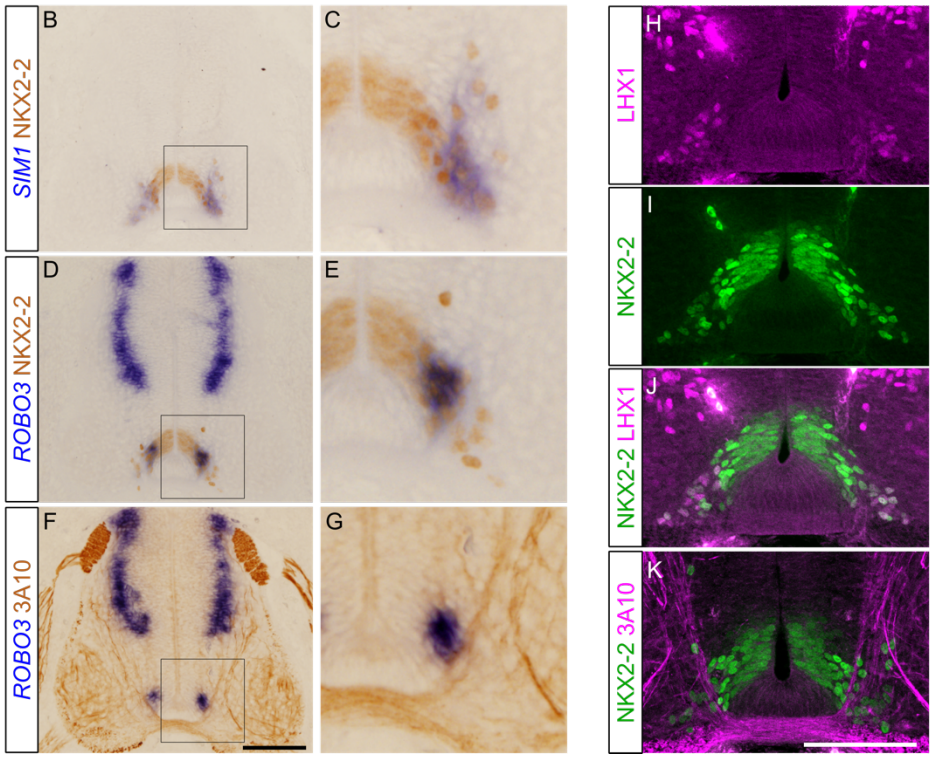
B
C
D
E
F
G
H
I
J
K
SIM1 NKX2-2
ROBO3 NKX2-2
ROBO3 3A10
LHX1
NKX2-2
NKX2-2 LHX1
NKX2-2 3A10

862 Figure 2

863

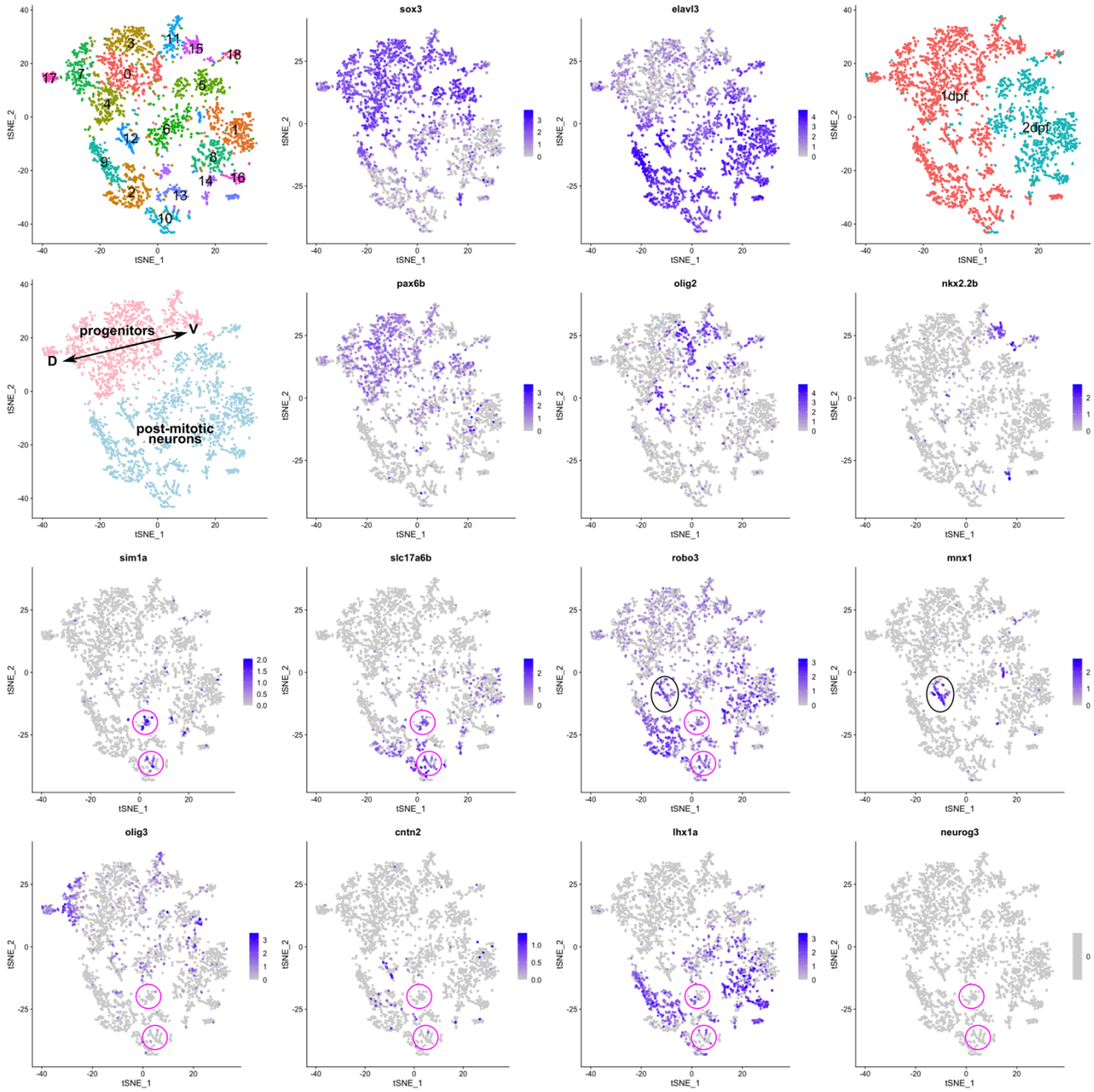

Figure 3

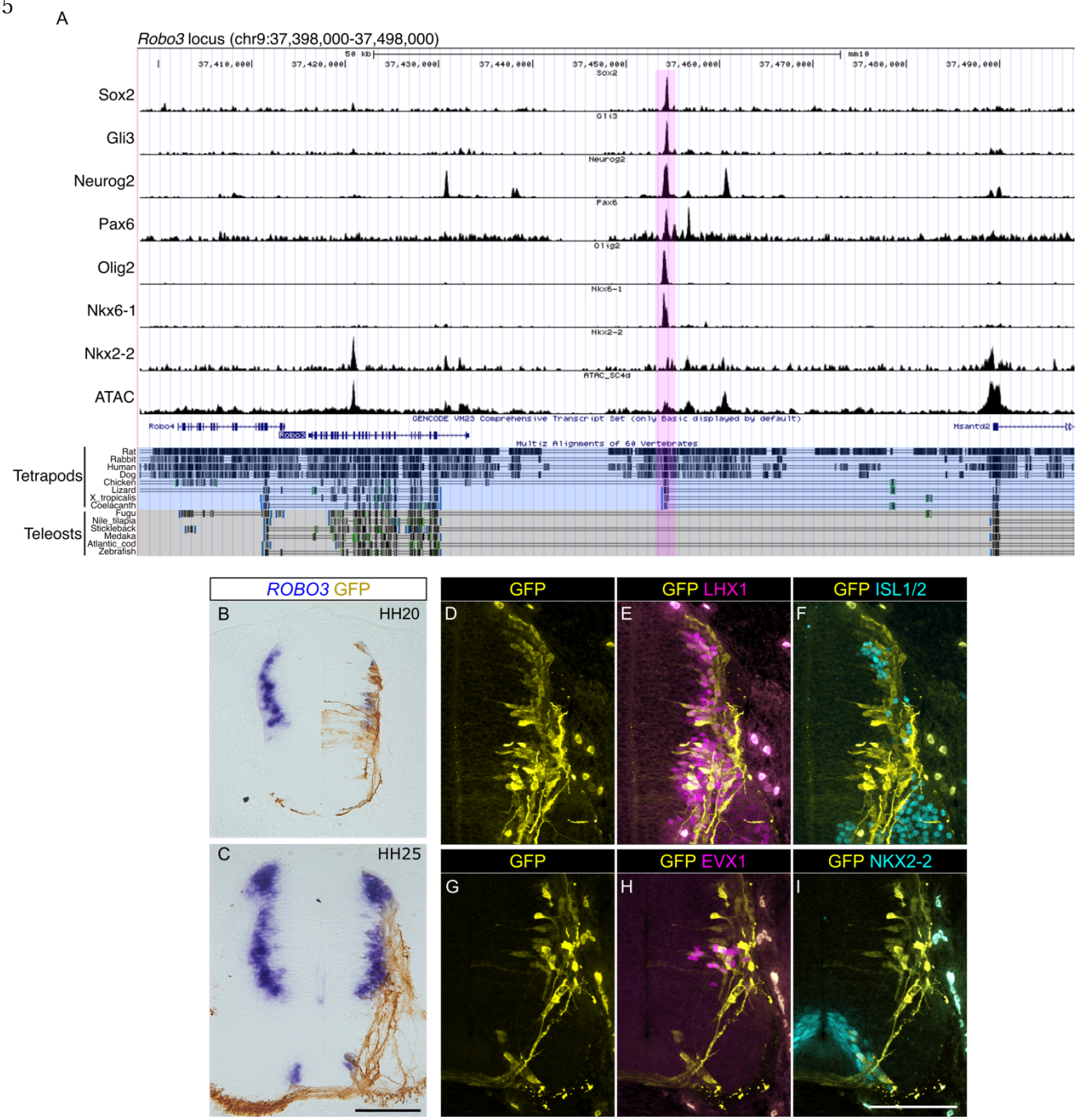
A
Robo3 locus (chr9:37,398,000-37,498,000)
Sox2
Gli3
Neurog2
Pax6
Olig2
Nkx6-1
Nkx2-2
ATAC
Tetrapods
Teleosts
ROBO3 GFP
B
HH20
C
HH25
GFP
GFP LHX1
GFP ISL1/2
D
E
F
GFP
GFP EVX1
GFP NKX2-2
G
H
I

866 Figure 4

867

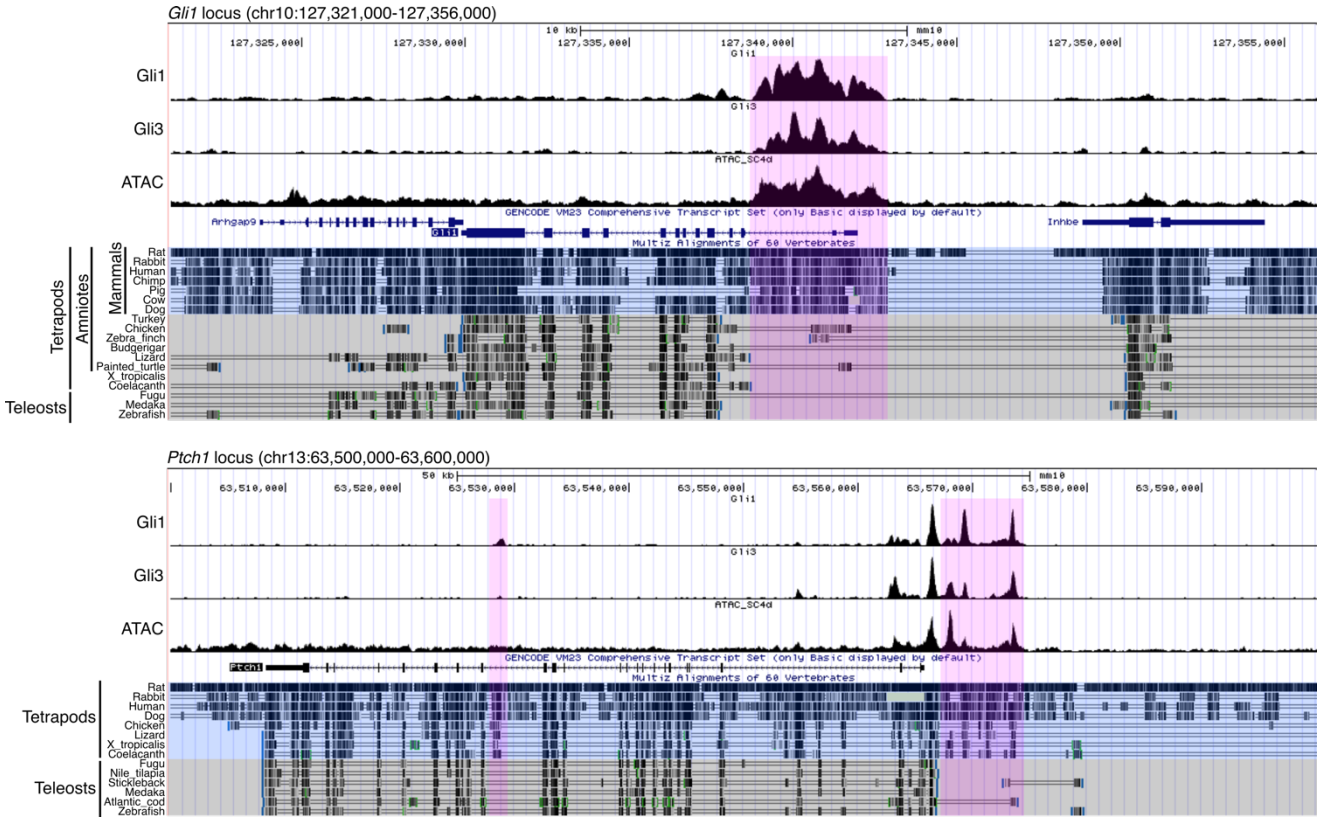

868 Figure 5

869

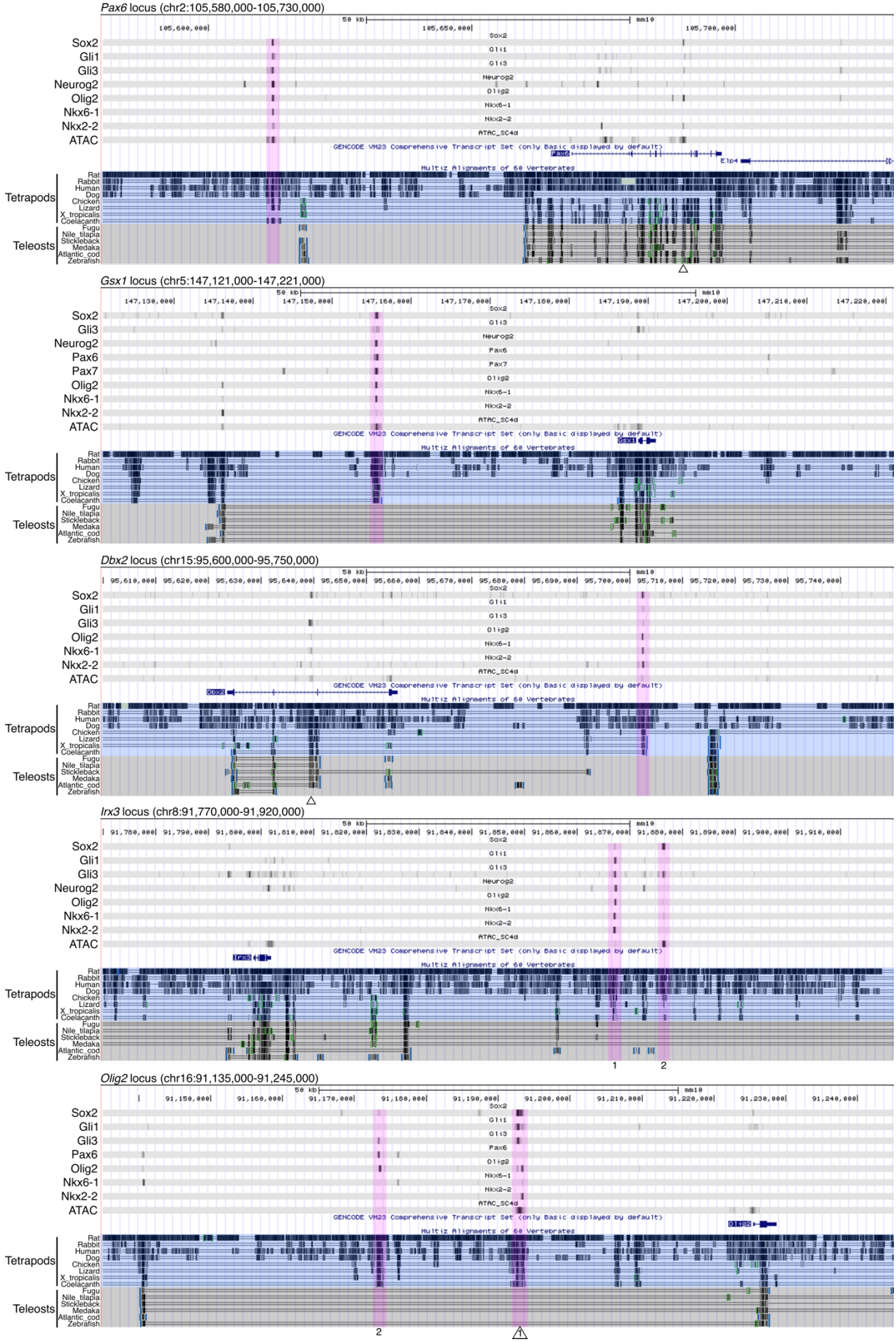

870 Figure 6

871

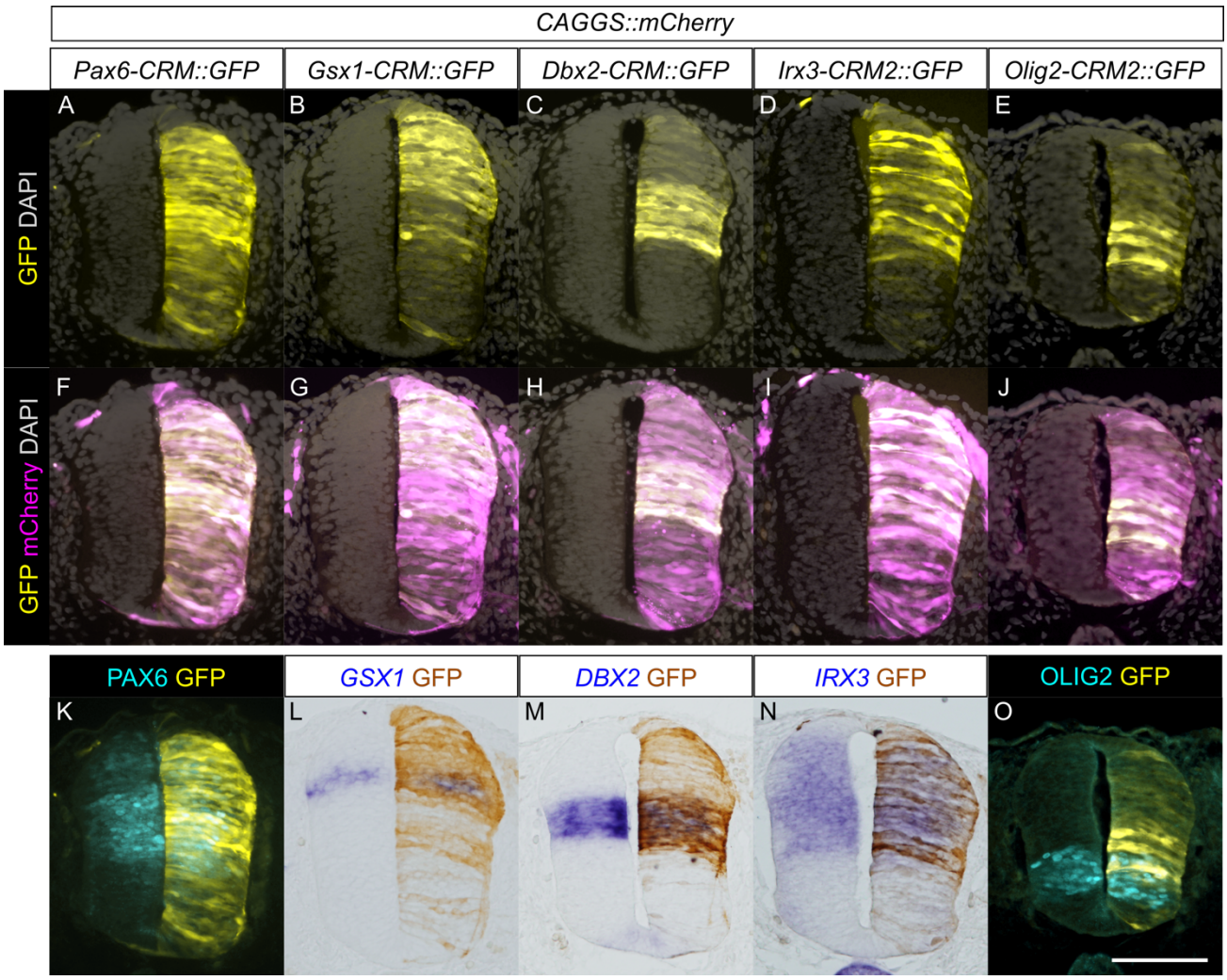

872 Figure 7

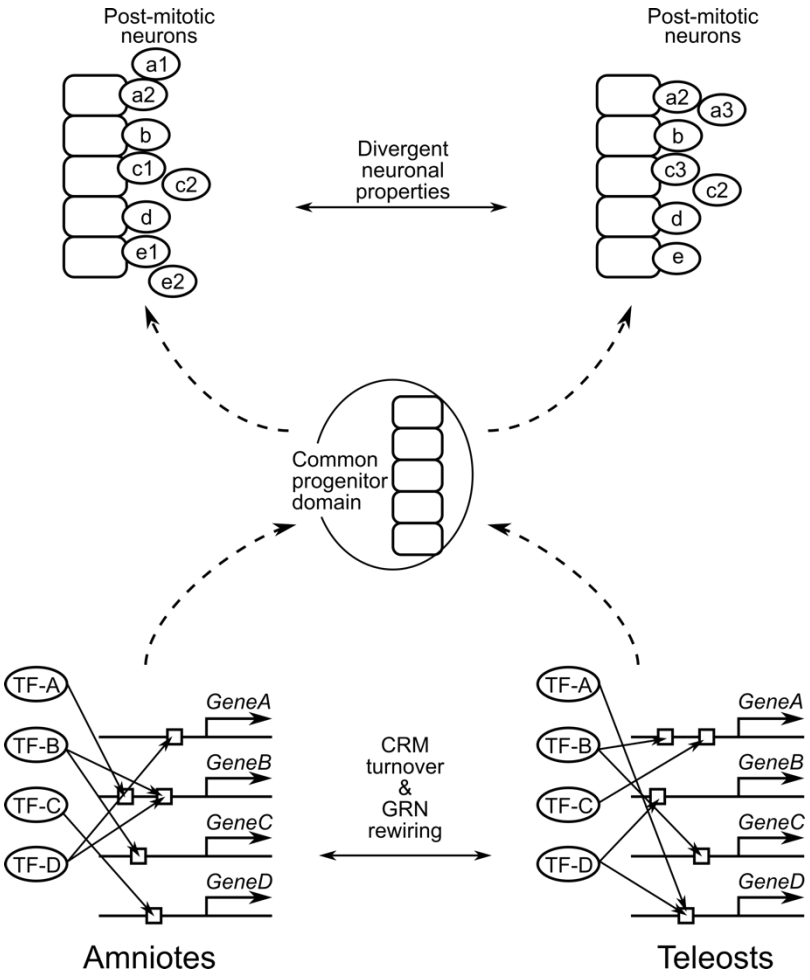
Post-mitotic neurons
a1
a2
b
c1
c2
d
e1
e2
Divergent neuronal properties
Post-mitotic neurons
a2
a3
b
c3
c2
d
e
Common progenitor domain
TF-A
TF-B
TF-C
TF-D
GeneA
GeneB
GeneC
GeneD
CRM turnover & GRN rewiring
TF-A
TF-B
TF-C
TF-D
GeneA
GeneB
GeneC
GeneD
Amniotes
Teleosts